

Analysis and Application of Sheppard's Airflow Model to Predict Mechanical Orographic Lifting and the Occurrence of Mountain Clouds

JAN KLEISSL AND RICHARD E. HONRATH

Department of Civil and Environmental Engineering, Michigan Technological University, Houghton, Michigan

DIAMANTINO V. HENRIQUES

Instituto de Meteorologia, Lisbon, Portugal

(Manuscript received 5 September 2005, in final form 2 February 2006)

ABSTRACT

Mechanically driven orographic lifting is important for air pollution dispersion and weather prediction, but the small dimensions of mountain peaks often prevent numerical weather models from producing detailed forecasts. Mechanical lifting in stratified flow over mountains and associated thermodynamic processes were quantified and evaluated using Sheppard's model to estimate the dividing-streamline height z_t . The model was based on numerical weather model profile data and was evaluated using ground-based measurements on a tall, axisymmetric mountaintop for which the nondimensional mountain height $h_{ND} = hN/U_\infty$ is frequently between 1 and 10 (here h is mountain height, N is Brunt-Väisälä frequency, and U_∞ is upstream horizontal wind speed). Sheppard's formula was successful in predicting water vapor saturation at the mountaintop, with a false-prediction rate of 14.5%. Wind speed was found to be strongly related to the likelihood of forecast errors, and wind direction, season, and stratification did not play significant roles. The potential temperature (water vapor mixing ratio) at z_t in the sounding was found to be slightly smaller (larger) than at the mountaintop, on average, indicating less lifting than predicted and/or turbulent mixing with higher-altitude air during parcel ascent. Detailed analysis revealed that this difference is a result of less lifting than predicted for small $U_\infty/(Nh)$, whereas Sheppard's model predicts the relative increase in uplift with increasing $U_\infty/(Nh)$ correctly for $U_\infty/(Nh) > 0.2$.

1. Introduction

Mountains and ridges influence atmospheric processes. Upslope flow near the surface of these obstacles is driven by buoyant forces (solar heating) or mechanical interaction of the flow with the barrier. This paper examines mechanical lifting in stratified flow over three-dimensional axisymmetric mountains. Ridges force air to travel either over or parallel to the ridge, whereas mountains or hills allow the flow to go over or laterally around them.

This paper focuses on the influence of mountains on airflow and the thermodynamic processes that occur during lifting. Most of the literature on flow around mountains has dealt with stably stratified dry air (e.g., Snyder 1985; Ding et al. 2003), either in the context of

air pollution dispersion [e.g., U.S. Environmental Protection Agency Complex Terrain Dispersion Model (CDTM; Perry et al. 1989)] or wind power use (e.g., Taylor and Teunissen 1987) or in the context of the calculation of the enhancement of precipitation as a result of orographic lifting of air near water vapor saturation (Miglietta and Buzzi 2001; Jiang 2003; Smith and Barstad 2004). The latter analyses are of particular interest to weather forecasting and hydrology. Most of this research has focused on wind-tunnel studies, towing-tank experiments, and numerical simulations. Only a small number of field studies have been conducted, mostly on small hills for which the initial height of a fluid parcel is hard to quantify because of small differences in potential temperature and water vapor mixing ratio over the height of the mountain (Jenkins et al. 1981; Spangler 1987; Taylor and Teunissen 1987).

Notable exceptions are very detailed studies of mountain meteorology that were conducted in the Alps [Mesoscale Alpine Program (MAP) experiment; e.g.,

Corresponding author address: Jan Kleissl, MTU, 1400 Townsend Dr., Houghton, MI 49931-1295.
E-mail: jan@kleissl.com

Bougeault et al. 2001] and on Hawaii Island [the Hawaiian Rainband Project (HaRP) experiment; Chen and Nash 1994]. The objective of the latter study was to find the cause responsible for flow blocking and the resulting rainband upwind of the island. However, the flow around Hawaii is of limited interest from a mechanical lifting standpoint because the nondimensional mountain height h_{ND} is typically greater than 2.5, which limits vertical motion ($h_{ND} = hN/U_\infty$, where h is the mountain height, N is the Brunt–Väisälä buoyancy frequency discussed below, and U_∞ is the upstream horizontal wind speed). In addition, because of the island's large size and the tropical location, buoyant effects caused by solar forcing (e.g., land–sea breezes) often dominate the flow regime (Carbone et al. 1995). In contrast, mechanical lifting is more prevalent on the island examined in this study because of its smaller size, higher latitude, and exposure to stronger winds, such that nondimensional mountain heights as low as 1 or lower are occasionally observed.

Numerical simulations (Ding et al. 2003), towing-tank studies (Snyder 1985; Hunt and Snyder 1980), field experiments (Trombetti and Tampieri 1987; Spangler 1987; Heinold et al. 2005), and linear theory (Smith 1989) have confirmed that the nondimensionalized mountain height is the most important parameter to classify stratified flows over mountains. The nondimensional mountain height has been interpreted as the reciprocal of a Froude number. See Baines (1995, p. 482) for a discussion of how the interpretation of h_{ND} differs from that of the Froude number. If the stratification is unstable, neutral, or weakly stable or the flow velocity is large, then all of the air will be lifted over the mountain. In this case, h_{ND} is said to be smaller than a critical nondimensional mountain height h_{ND}^{crit} , with h_{ND}^{crit} being $O(1)$ (Smith and Gronas 1993; Baines and Smith 1993). If $h_{ND} > h_{ND}^{crit}$, upstream blocking will occur as follows. As stable low-level air is pushed up the windward slope, it becomes colder than air at the same level. This creates high pressure near the slope that decelerates or even reverses the incoming flow (Smith 1989). In the case of blocking, the upstream air column can then be divided into two parts, with the lower part traveling around the mountain and the upper part traveling over the mountain. The streamline separating these two parts is termed the dividing streamline, and its height upstream of the mountain is termed z_t (Fig. 1). An air parcel above the dividing streamline will flow over the mountain, and air parcels below the dividing streamline will be lifted but will eventually flow around the mountain. [Some authors have defined the dividing streamline differently, as discussed by Ding et al. (2003).] If condensation occurs from lifting of moist air, the result-

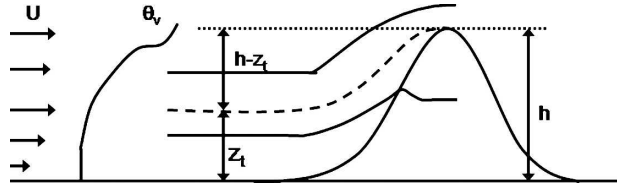


FIG. 1. Schematic graph of orographic lifting over a mountain peak. Here, U is the horizontal velocity profile, θ_v is the virtual potential temperature profile, z_t is the dividing-streamline height, and h is the mountain height.

ing latent heat release drives additional lifting and reduces the dividing-streamline height (Miglietta and Buzzi 2001).

Three main theories have been developed to describe the flow field around mountains as a function of nondimensional mountain height. Drazin's (1961) potential-flow theory is applicable to large h_{ND} and predicts that fluid parcels remain in horizontal planes as they move around the mountain. Considering small h_{ND} , Smith (1980) introduced linear theory by linearizing the hydrostatic equations of motion and solving for the hill-induced velocity, density, and pressure perturbation fields. He postulated that the linearized equations of motion are accurate for $h_{ND} < 1$ only, but Smolarkiewicz and Rotunno (1990) showed that the solution to the linearized equations of motion provides meaningful predictions down to the incipient stagnation. According to the solution to the linearized equations of motion, at $h_{ND}^{crit} = 1.3$ a stagnation point will form on the upwind surface of a Gaussian hill. Although linear theory can be applied to determine the existence and location of an upwind stagnation point, it is only of limited value for determining the lifting of air that reaches the mountaintop for the most interesting dynamic regime $h_{ND} \geq 1$. This is due to both the breakdown of linear theory for $h_{ND} \approx 1$ and the lower boundary condition for the vertical displacement η of density surfaces relative to their upwind height. At the hill surface $h(x, y)$, this lower boundary condition is typically chosen as $\eta(x, y, z = h) = h(x, y)$, which implies that the vertical displacement of a fluid parcel reaching the summit is always equal to the height of the hill, independent of h_{ND} . This is not problematic for the range of applicability of linear theory, since for $h_{ND} < 1$ all air is expected to flow over the mountain, but is problematic for $h_{ND} > 1$ when parts the upstream air column are expected to flow around the obstacle (Smith 1988).

A third theory based on Bernoulli's equation (Sheppard 1956) has proven to be successful for predicting the degree of lifting in a variety of studies (e.g., Hunt and Snyder 1980; Vosper et al. 1999; Ding et al. 2003). Sheppard postulated that along a streamline kinetic en-

ergy is converted to potential energy as fluid parcels rise over the hill. The dividing-streamline height is calculated as the upstream height of the streamline for which kinetic energy reaches zero at the summit of the mountain. Sheppard's model is described further in section 2a.

In this paper we compute the thermodynamics (temperature, pressure, and water vapor mixing ratio) of a fluid parcel on the dividing streamline (as predicted by Sheppard) and compare them with meteorological observations on a mountaintop. Several field experiments have exploited the fact that unsaturated air may become saturated and form clouds ("flow-through reactors") as it flows over a mountaintop, returning to an unsaturated state again when it descends the mountain (e.g., Heinold et al. 2005; Colvile et al. 1997). However, most such studies focused on the chemical composition of air rather than on quantifying the amount of lifting. Leung and Ghan (1995) coupled a simple airflow model to a thermodynamic model to quantify subgrid-scale orographic rainfall for coarse-grid numerical weather and climate models. They found high correlations between the spatial distribution of observed and simulated rainfall in the state of Washington during the winter months (stratiform clouds) but almost no correlation in the summer months (cumuliform clouds). Rainfall prediction is more difficult than prediction of water vapor saturation (as attempted in this paper) because complex microphysical processes (besides orographic lifting) control orographic precipitation (Barros and Lettenmaier 1994). In addition, a time lag (and a space lag) between cloud formation and rainfall have to be taken into account.

In summary, despite a great amount of research on stratified flow over hills, few field studies have quantified mechanically driven orographic lifting on tall mountains. A better understanding of mechanically driven orographic lifting is needed for several reasons. It is important for air pollution dispersion and weather prediction, but the small dimensions of mountain peaks often prevent detailed forecasts by weather and climate models. In addition, parameterizations for orographic rain based on Sheppard's model are useful for numerical weather prediction and climate models (Leung and Ghan 1995). Last, water vapor saturation is a good proxy to predict clouds, which is of great practical importance for mountaineers and aviators. In this paper we address this need by evaluating Sheppard's model with measurements on an isolated, tall, axisymmetric mountain, which is frequently exposed to strong winds.

The remainder of this paper is composed as follows. We describe the methods and data utilized in this study in section 2. In section 3, we apply Sheppard's model to

compute the dividing-streamline height. We then assume conservation of potential temperature and water vapor mixing ratio during parcel ascent to predict the lifting condensation level of air originating from the dividing-streamline height and compare the results with concurrent relative humidity readings from the mountaintop to test Sheppard's model. Section 4 contains the conclusions.

2. Data and analysis procedures

a. Sheppard's model

Sheppard (1956) postulated that the maximum amount of vertical lifting undergone by fluid parcels that travel over the mountaintop can be iteratively determined from

$$\frac{1}{2} U_{\infty}^2(z_t) = \int_{z_t}^h (h - z) N^2(z) dz, \quad (1)$$

where $N^2 = g/T_v \partial \theta_v / \partial z$ is the Brunt-Väisälä frequency squared, $T_v(z)$ is the virtual temperature, $\theta_v(z)$ is the virtual potential temperature, and z_t is the height of the dividing streamline, the lowest initial height of air parcels that travel over the mountaintop (Fig. 1). In the case of constant $U_{\infty}(z)$ and constant $N(z)$, the equation simplifies to $z_t = h[1 - U_{\infty}/(Nh)]$ (Sheppard's formula). Thus, the air that reaches the mountaintop has been lifted by $h - z_t = U_{\infty}/N$. In the following we will refer to Eq. (1) as Sheppard's model, whereas the term "Sheppard's formula" will refer to the simplified expression. Sheppard's model is used for all calculations presented below.

The following assumptions underlie Eq. (1). First, Sheppard (1956) assumed that the flow is inviscid and that the velocity and pressure fluctuation at the summit of the hill are zero; that is, the kinetic energy upstream has been completely converted to potential energy when the fluid parcel reaches the summit. This assumption is false. For example, linear theory predicts that speed variations are associated only with nonlocal hydrostatic pressure variations and not with local parcel lifting (Smith 1989). Linear theory and 3D numerical simulations have revealed that stagnation occurs first on the windward slope (e.g., Olafsson and Bougeault 1996), and the wind speed at the summit can be even larger than upwind because of convergence of streamlines. Nonlinear effects such as stagnation and reverse flow on the windward slope and wave breaking above the lee slope are important to predict upstream blocking (e.g., Smolarkiewicz and Rotunno 1990) but are not considered in Sheppard's model. However, Ding et al. (2003) demonstrated that for inviscid flow Sheppard's

formula is successful because “the energy provided by pressure field roughly offsets the energy loss due to friction/turbulence for axisymmetric hills.”

Second, the rotation of the earth—that is, the Coriolis force—is neglected. This limits the applicability of the analysis to small-scale mountains or large Rossby numbers $Ro = U_\infty/(fL)$, where L is the mountain half-width and f is the Coriolis parameter. Larger mountains are resolved by NWP and climate models, and so this is not a serious limitation. Smith (1980) suggested that the Coriolis force can be neglected for mountain widths of less than 50 km; more recent studies examine the behavior of the flow at different Rossby numbers in more detail (e.g., Grisogono and Enger 2004). For the significant wind speeds needed to cause mechanical lifting ($>1 \text{ m s}^{-1}$), Rossby numbers for flow around Pico Mountain in the Azores Islands of Portugal are greater than 10.6, indicating only weak effects of the Coriolis force (L was measured as one-half of the largest width of the mountain at $z = 1112 \text{ m}$).

Third, the influence of the shape of the mountain is neglected. Shape and slope of the mountain are of importance. For example, with a slope of 1 (a vertical building) only negligible lifting occurs, whereas surfaces with a slope between 0 and 1 cause various amounts of lifting. Most experimental work has focused on Gaussian hills, for which Eq. (1) has been shown to be in good agreement with observations (Hunt and Snyder 1980). Vosper et al. (1999) studied different three-dimensional obstacles (hemispheres and cones) and found that, for the same h_{ND} , the lifting over cones was less than that over hemispheres. They argue that a small velocity component perpendicular to the mean flow in the upstream velocity field has a greater influence on obstacles with a narrow top (such as cones), causing the flow to travel over the shoulder of the obstacle rather than over the summit. This finding might be important for flow over tall mountains, since the upstream wind direction often varies with height. Effects of hill shape on the flow field around mountains have also been studied using linear theory (Smith 1989). Last, Eq. (1) does not account for moist thermodynamics such as latent heating from condensation or latent cooling from evaporating orographic rain, unless an equivalent moist buoyancy frequency is used (Jiang 2003).

b. Mountaintop station and sounding data

The lifting calculations in the following sections were evaluated with a dataset from Pico Mountain (Fig. 2). Pico Mountain is a volcanic mountain with a nearly ideal conical shape and an average slope of $\sim 45\%$

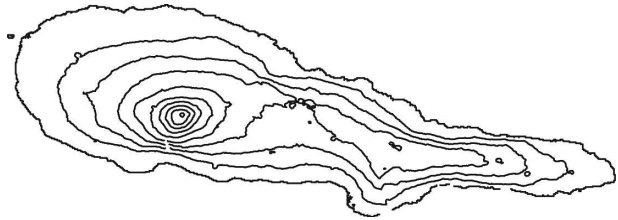


FIG. 2. Topographical map of Pico Island from Shuttle Radar Topography Mission data (National Aeronautics and Space Administration and U.S. Geological Survey; at the time of writing information was available online at <http://seamless.usgs.gov>). Contours are spaced 250 m apart, from 0 to 2250 m. The east–west and north–south dimensions of the island are 45 and 20 km, respectively. The PICO-NARE station is located at 38.47°N , 28.40°W at 2225 m, just northwest of the summit. Most of the terrain above 1250 m is bare lava soils; most lower-lying areas are grasslands.

above $z \sim 1250 \text{ m MSL}$. There is little vegetation other than short groundcover on the mountain above 1250 m, and most of the surface consists of bare lava rock or gravel. Pico Island is approximately 45 km long and 15 km wide. The upwind distance that air travels over the island before reaching the mountaintop is 7–13 km for the most common wind directions (between southwest and north). The Pico International Atmospheric Chemistry Observatory (PICO)-North Atlantic Regional Experiment (NARE) station is located near the summit ($z = 2225 \text{ m}$; 38.47°N , 28.40°W ; Honrath et al. 2004), 50 m from the north end of a flat, circular caldera with a diameter of $\sim 500 \text{ m}$. Meteorological variables and trace gas concentrations have been monitored since July of 2001 to study background levels and the trans-Atlantic transport of air pollution. Temperature and relative humidity were measured at 3 m AGL by a Rotronic Instrument Corporation Hygroflex TM12R that was purchased new in 2001. In the summer of 2002, it was destroyed by adverse weather and was replaced with a new Rotronic Hygroflex M1. In the summer of 2004, that second sensor was intercompared with another new sensor and was found to be within the specifications (accuracies of 1% RH and 0.3°C). No time dependence of the results presented in this paper was found, which confirms that the sensors operated properly. Atmospheric pressure was measured by an R. M. Young Company 61201 barometric pressure sensor. Intercomparisons with radiosonde data indicated that the pressure sensor operated within specifications (accuracy of $\pm 2.0 \text{ hPa}$). This accuracy is somewhat low, but it does not affect the mountain cloud model evaluation, because these pressure readings are used neither for model prediction nor for the primary model evaluation (which relies on RH measurements only). Pressure is used to calculate θ_e and water vapor mixing ratio q at

the station. On average, an inaccuracy of ± 2.0 hPa translates to ± 0.22 K for θ_v and $\pm 15 \times 10^{-3}$ g kg $^{-1}$ for q , both of which are an order or magnitude less than the observed differences between the mountaintop measurements and the European Centre for Medium Range Weather Forecasts (ECMWF) value at the dividing-streamline height (discussed below).

To determine lifting, measurements at the mountaintop should be compared with vertical soundings upstream of the mountain. Vertical profiles of the Brunt-Väisälä frequency $N(z)$, water vapor mixing ratio $q(z)$, and wind speed $U_\infty(z)$ can be obtained from radiosoundings from the nearby island of Terceira (World Meteorological Organization identification number = 08508, 38.73°N, 27.07°W, 119 km at a bearing of 75° from Pico; information obtained online at <http://raob.fsl.noaa.gov>) or from the ECMWF global numerical weather model (0.5° latitude \times 0.5° longitude resolution, 6 hourly; information was available online at <http://www.ecmwf.int>). We used the ECMWF reanalysis dataset (ERA40) until August of 2002 and the operational model (T511) thereafter. The radiosonde data have several disadvantages: There are, on average, only 1.4 soundings per day; wind data are often missing (in 45% of the soundings); the release location is displaced from Pico Mountain by 119 km; and the data present only an instantaneous depiction of the state of the atmosphere. These shortcomings led us to choose ECMWF data for this analysis. Note that, because the horizontal resolution of ECMWF is ~ 50 km, Pico Island represents subgrid-scale terrain. Thus the profiles obtained from ECMWF at Pico Mountain are representative of conditions upstream of the island. From the EMCWF archives, $T(p)$, $q(p)$, $U(p)$, and geopotential height were obtained at 18 vertical levels between the surface and 700 hPa and horizontally interpolated from the four surrounding grid points to Pico.

Lifting predictions were analyzed using 30-min averages of relative humidity RH_{PICO} and virtual potential temperature $\theta_{v,\text{PICO}}$ from the PICO-NARE station. Times when $T_{\text{PICO}} < 0^\circ\text{C}$ were not considered because the sensors are not well ventilated in these conditions as a result of frequent heavy icing. Saturated water vapor conditions were assumed when the 30-min-averaged $RH_{\text{PICO}} > 98\%$. A visual examination of 6-hourly photographs taken at the PICO-NARE station indicates that this criterion is a good proxy for cloud formation. Because of extended station and sensor down times and occasional conditions in which $T_{\text{PICO}} < 0^\circ\text{C}$, the total number of observations synchronized to the sounding data was 2479 six-hourly observations, corresponding to a data coverage of 48% for the 3.5-yr period.

c. Computing the dividing-streamline height and nondimensional mountain height

Although the airflow model of Eq. (1) can be applied for any velocity and temperature profile, computing the nondimensional mountain height $h_{\text{ND}} = hN/U_\infty$ implicitly assumes constant $N(z)$. In the following, the average N between z_t and h and the upstream velocity at the dividing-streamline height [$U_\infty(z_t)$; Spangler 1987] were used to compute h_{ND} , and z_t from Sheppard's model was obtained from Eq. (1) (h_{ND} is not used to derive the predictions presented below, but is used as the independent variable in some plots analyzing the predictions).

d. Computing the lifting condensation level

In section 3, water vapor saturation (as a proxy for cloud formation given sufficient abundance of cloud condensation nuclei) will be predicted. The lifting condensation level (LCL) of an air parcel is the height at which the parcel's relative humidity will reach 100%, if it is lifted adiabatically and without mixing. Using Sheppard's airflow model [Eq. (1)] we computed the LCL of an air parcel originating at the dividing-streamline height z_t as follows. When given ambient temperature T , dewpoint temperature T_d , and pressure p at height z_t , the LCL is the altitude in the skew T - $\log p$ diagram at which the dry adiabat through $T(z_t)$ intersects the mixing-ratio line through $T_d(z_t)$. The dry adiabat through $T(z_t)$ is given by

$$T^{\text{da}}(z) = T(z_t) \left[\frac{p(z)}{p(z_t)} \right]^{R_d/c_{p,m}(z_t)}, \quad (2)$$

where $R_d = 287$ J kg $^{-1}$ K $^{-1}$ is the gas constant for dry air, $c_{p,m} = 1005.7(1 + 0.85q)$ J kg $^{-1}$ K $^{-1}$ is the specific heat of moist air at constant pressure, and q (kilograms of H $_2$ O per kilogram of air) is the water vapor mixing ratio. The line of dewpoint temperature for constant q (the mixing-ratio line) is defined by the empirical formula

$$T^{\text{mr}}(z) = [b - (b^2 - 223.1986)^{1/2}]/(0.018\,275\,804\,8\text{ K}^{-1}), \quad (3)$$

where

$$b = 26.660\,82 - \ln[e(z)] \quad \text{and} \\ e(z) = p(z)q(z_t)/[0.622 + q(z_t)] \quad (4)$$

Parameter $e(z)$ (hPa) is the pressure of water in air originating at z_t and lifted to height z , and p (hPa) is the pressure. Mixing ratio q is conserved during parcel ascent. Temperature $T^{\text{mr}}(z)$ describes the temperature to which an air parcel that has risen adiabatically from z_t

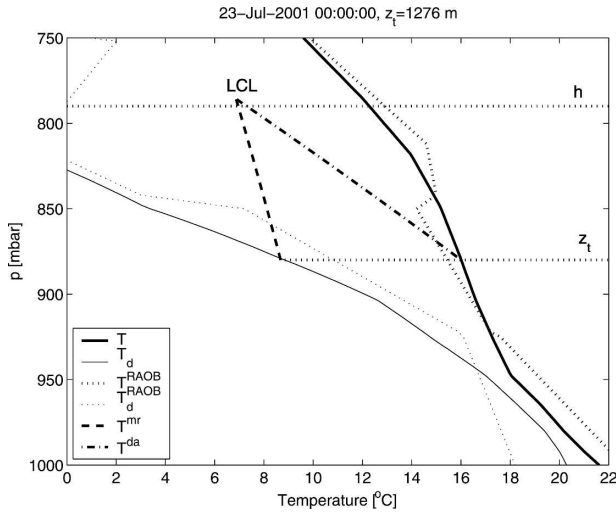


FIG. 3. Sample vertical profiles with depiction of the LCL of air originating from the dividing-streamline height ($z_t = 1276$ m at $p = 880$ hPa). The mountain height $h = 2225$ m ($p = 790$ hPa) is shown as a dotted line. Temperature T and dewpoint temperature T_d are shown for ECMWF data at 0000 UTC 23 Jul 2001 (solid lines) and a radiosounding from Terceira at 2300 UTC 22 Jul 2001 (dotted lines). Here, T^{mr} is the line of dewpoint temperature for constant water vapor mixing ratio defined by Eq. (3) and T^{da} is the dry adiabat defined by Eq. (2).

to z has to be cooled for saturation to occur. These equations were taken from the Advanced Weather Interactive Processing System (accessed online at <http://meted.ucar.edu/awips/validate/skewT2t.html> on 28 April 2005). We obtained the LCL by finding the height at which $T^{da}(z) = T^{mr}(z)$.

3. Application and evaluation of Sheppard's model

In absence of liquid water, diabatic rise, and mixing, virtual potential temperature θ_v , and water vapor mixing ratio q_v are conserved during parcel ascent. In this section, we exploit these conservation laws to test the prediction of Sheppard's model for the amount of lifting, $h - z_t$ [Eq. (1)].

a. Water vapor saturation prediction on mountaintops based on Sheppard's model

Because mechanical lifting in mountainous terrain is often associated with clouds ("upslope fog") and rain, which are of great practical relevance to aviators, mountaineers, weather forecasters, and hydrologists, we investigated how well Sheppard's formula coupled to a thermodynamic model can predict saturated conditions on mountaintops.

To do this, we first computed the amount of lifting using Eq. (1) and the ECMWF vertical profile data.

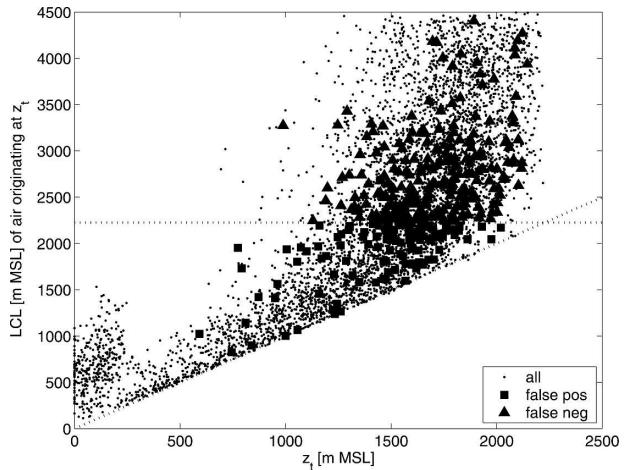


FIG. 4. Predicted LCL and dividing-streamline height z_t determined from Eq. (1) and thermodynamic equations described in section 2d. Dots are correctly predicted data, squares indicate that saturation was predicted but not observed (false positives), and triangles indicate that no saturation was predicted but saturation was observed (false negatives). The diagonal dotted line shows $LCL = z_t$. Lengths are not normalized by $h = 2225$ m so that the actual dimensions can be visualized.

Second, we quantified the change in thermodynamic properties to compute the LCL of an air parcel at z_t . This tells us whether the decrease in temperature [determined from Eq. (2)] and a smaller decrease in dewpoint temperature [Eq. (3)] lead to water vapor saturation during lifting from z_t to h . Figure 3 shows an illustration of the temperature and dewpoint that an air parcel would follow during mechanical lifting. The intercept between the dot-dashed and dashed lines is the LCL of air originating at z_t (in this case, $z_t = 1276$ m). By comparing $LCL(z_t)$ with h , the presence or absence of water vapor saturation at the mountaintop was predicted. The predictions from the model for $LCL < h$ (saturation) or $LCL > h$ (no saturation) were compared with relative humidity measured on the mountaintop. In the example shown in Fig. 3 the LCL is just above h , and therefore water vapor saturation would not be expected to occur during the rise to the mountaintop. The figure also shows a radiosounding from nearby Terceira, which agrees well with the ECMWF profiles at Pico.

We determined dividing-streamline height z_t and LCL for all 2479 ECMWF vertical profiles. Figure 4 depicts a scatterplot of LCL versus z_t for each vertical profile. The dividing-streamline height as obtained from Eq. (1) is bounded between zero (all air is lifted over the mountain) and the mountain height h (no air is lifted over the mountain). For each possible z_t a range of LCLs is observed. The LCL is bounded by z_t as a

TABLE 1. Number of occurrences of saturated conditions in the model forecast vs observed $RH_{PICO} > 98\%$ at $h = 2225$ m. Each prediction type is given in parentheses: cp is correct positives, fp is false positives, fn is false negatives, and cn is correct negatives.

Saturation predicted	Saturation observed			
	Yes		No	
	No.	%	No.	%
Yes	681 (cp)	86	112 (fp)	14
No	248 (fn)	15	1436 (cn)	85

lower bound and 4500 m as an artificially introduced upper bound (in theory LCL could be larger than that, but the exact value is of no interest here once it is significantly larger than h). Data points whose prediction for saturation is confirmed by the RH measurement at the mountaintop are shown as dots, and wrongly predicted data points are shown as squares if $LCL < h$ (predicted saturated) and triangles if $LCL > h$ (predicted unsaturated). The LCLs of wrongly predicted data are concentrated around h , indicating that a small change in predicted LCL would suffice for a correct prediction.

During the analysis of these predictions the nomenclature of hypothesis testing is utilized. If no saturation was predicted ($LCL > h$) and no saturation was observed ($RH_{PICO} < 98\%$), the prediction is termed a correct negative (shown as dots above $y = h$ in Fig. 4). If saturation was predicted ($LCL < h$) and saturation was observed ($RH_{PICO} > 98\%$), the prediction is termed a correct positive (shown as dots below $y = h$ in Fig. 4). On the other hand, if saturation was predicted ($LCL < h$) but no saturation was observed ($RH_{PICO} < 98\%$), the prediction is termed a false positive (shown as squares in Fig. 4). In a similar way, if no saturation was predicted ($LCL > h$) but saturation was observed ($RH_{PICO} > 98\%$), the prediction is termed a false negative (shown as triangles in Fig. 4).

Table 1 summarizes the number of observations and the frequency of each prediction–observation pair. The saturation prediction model based on Sheppard’s formula has high sensitivity (correct positives divided by the sum of correct positives and false negatives is 73%) and very high specificity (correct negatives divided by the sum of correct negatives and false positives is 92%). Interpreting the results from the point of view of the model, the no-saturation predictive value is 85% (when no saturation is forecast, the likelihood of observed saturation is low: 15%). The saturation predictive value is 86% (when saturation is forecast the likelihood that no saturation is observed is equally low: 14%).

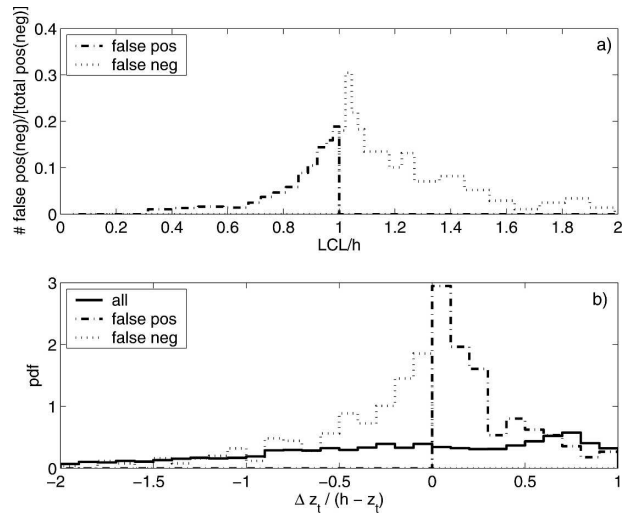


FIG. 5. Distribution of false-positive and false-negative predictions. (a) Fraction of false predictions as a function of the LCL of air originating from z_r . (b) Probability density function of the difference between the height $z_r^{LCL=h}$ of the streamline that becomes saturated exactly at the mountaintop and the predicted z_r ($\Delta z_r = z_r^{LCL=h} - z_r$).

b. Analysis of the distribution of prediction errors of Sheppard’s model and quantification of uncertainties

Our analysis targets orographic clouds, but false-negative predictions could also be the result of advection of frontal or convective clouds to the mountaintop in light wind conditions, when no condensation was forecast by Sheppard’s model. To test whether the advection of nonorographic clouds caused false-negative predictions, we looked at time periods in which the Aviation Routine Weather Report (METAR) from Horta in the Azores (LPHR) indicated cloud bases at an altitude between 2000 and 2300 m. This condition occurs approximately 12% of the time. Clouds at this location and altitude are usually not orographic because of the large distance of the METAR station from Pico Mountain. During time periods with observed clouds over Horta, the ratio of false-negative predictions divided by correct-positive predictions was not larger than that for the entire dataset. This result indicates that advection of nonorographic clouds to the mountaintop is not a likely explanation for false-negative observations.

To explore the reasons for false predictions, we first examined the dependence of the false-positive and false-negative predictions upon small changes in z_r . Figure 5a shows the fraction of false observations as a function of LCL. The fraction of false observations clearly peaks as LCL becomes similar to h . Near LCL =

TABLE 2. Means and medians of Δz_i (the change in z_i required to obtain LCL equal to h), in meters and normalized by the predicted uplift ($h - z_i$), for false positives and false negatives.

Type	$\Delta z_i/(h - z_i)$		Δz_i (m)	
	Mean	Median	Mean	Median
False positive	0.29	0.20	243	133
False negative	-0.83	-0.40	-253	-204

h the fraction of false negatives is larger than the fraction of false positives. This result indicates that the actual lifting for the data points with LCL near h is, on average, more than that predicted by Eq. (1), since more lifting (smaller z_i) would lead to a smaller LCL. Thus an increase in lifting would move the LCL of some false-negative data points below h to make them correct positives while at the same time moving the LCL of some correct negative data points below h to make them false positives. If the ratio of false negatives to correct negatives in the subset of data points whose LCL becomes smaller than h is larger than the overall false-prediction rate, then it will lead to an overall improvement of the success rate of the model. Maximization of the overall success rate is discussed further below.

Because the difference between LCL and z_i varies depending on the temperature and dewpoint temperature at z_i , the change in LCL required to obtain correct predictions (Fig. 5a) does not directly indicate the error in predicting z_i . Figure 5b shows the change in z_i required to obtain an LCL equal to h . (For the false predictions, this is the minimum change in z_i required to obtain a correct prediction.) The medians of the false-positive and false-negative distributions are 0.2 and -0.4, respectively; that is, more than 50% of the false positives would be correct negatives if the actual lifting were 20% smaller than predicted, and more than 50% of the false negatives would be correct positives if the actual lifting were 40% larger than predicted. The means and medians of the false positives and false negatives are given in Table 2. Figure 5 also shows the distribution of $\Delta z_i/(h - z_i)$ for all predictions. Unlike the distributions of false predictions, the overall distribution is fairly uniform over the range in which most false predictions occur.

Because this paper uses data from numerical weather models and involves field data, an estimation of uncertainties is appropriate. Errors in the ECMWF data stem from poor temporal and vertical resolution and forecast error over an area for which only sparse surface and sounding data are available for assimilation. The flow over the mountain is influenced by turbulent mixing, pressure forces, and temperature differences between

the mountain and the overlying air, none of which is taken into account by Sheppard's model. An estimate of the magnitude of the cumulative error from sounding data, nonideal field conditions, and model error can be obtained from the distribution of all false predictions (the union of the dotted and dot-dashed lines shown in Fig. 5b). If we assume that the error in the prediction for z_i is normally distributed [$(z_i - z_i^{\text{Sheppard}})/(h - z_i) = \epsilon$, $\epsilon \in \mathcal{N}(0, \sigma)$], the standard deviation σ can be determined by fitting a normal distribution \mathcal{N} to the probability density function of false predictions in Fig. 5b. The standard deviation is $\sigma = 0.38$, indicating a 38% error in the prediction for lifting.

To allow comparison with an alternative numerical model, we also repeated this analysis, using results from the final run (FNL) of the Global Data Assimilation System global numerical weather model (190-km horizontal spacing; vertical data points at 1000, 925, 850, and 700 hPa; 6 hourly; at the time of writing, information was available online at http://www.arl.noaa.gov/NOAAserver/FNL_info.html). Despite the coarser model resolution, the predictive value of the model was only moderately degraded. Using FNL data, the non-saturation predictive value was 87% and the saturation predictive value was 76% (as compared with 84%–85% with ECMWF data), and the overall false prediction rate was 16.9% (as compared with 14.7% with ECMWF data).

c. Adjusting Sheppard's model for optimum performance

For practical purposes we briefly present how Sheppard's model could be adjusted to yield optimum performance—that is, the smallest fraction of total false predictions. To achieve this goal for the study presented here, the amount of lifting must be increased to produce fewer false negatives with slightly more false positives. We introduced a factor α^2 in Sheppard's model that multiplies the left-hand side of Eq. (1) to give

$$\frac{1}{2} \alpha^2 U_\infty^2(z_i) = \int_{z_i}^h (h - z) N^2(z) dz. \quad (5)$$

For $\alpha > 1$, it can be thought of as an artificial increase of the kinetic energy of the flow, equivalent to changing Sheppard's formula to $z_i/h = 1 - \alpha U_\infty/(Nh)$. In the modified Sheppard's formula, α describes the slope and the inverse of the x intercept of the lifting line in a graph of z_i/h versus $U_\infty/(Nh)$ (see Fig. 6). Thus α is equal to the largest $U_\infty/(Nh)$ for which not all air flows over the mountain, also referred to as the onset of stagnation. [Because $\alpha = 1$ in Sheppard's original formula,

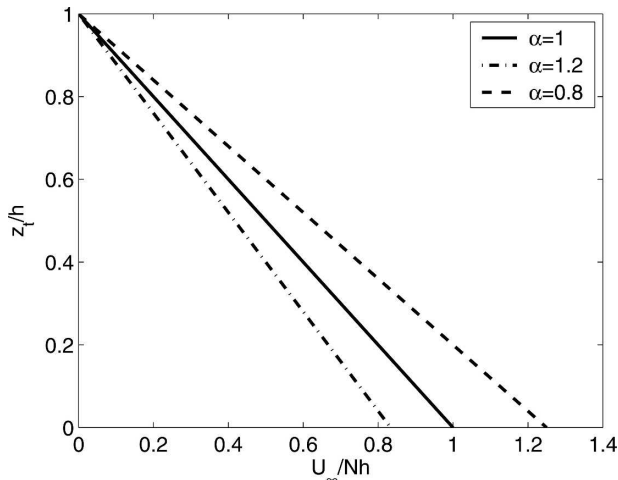


FIG. 6. Dividing-streamline height predicted from Sheppard's formula for different values of α .

stagnation is predicted to occur at $U_\infty/(Nh) = 1$.] Factor α was introduced by Drazin (1961) to account for the shape of the hill. It can also be thought of as a lumped parameter that accounts for the deficiencies in Sheppard's model outlined in section 2a. Hunt and Snyder (1980) found $\alpha = 1$ was the best fit to their laboratory data on a circular mountain, and Olafsson and Bougeault (1996) obtained $\alpha = 1.2$ from numerical simulations of flow over a ridge with an aspect ratio of 5.

By varying α , we found that $\alpha = 1.16$ results in the minimum total false-prediction rate at 13.9%. At this value of α , the ratio of false positives divided by the sum of false positives and correct negatives is 11% and the ratio of false negatives divided by the sum of false negatives and correct positives is 18%. Thus the lifting that results in the optimum total false-prediction rate is slightly more (16%) than is predicted by Eq. (1). Because the total false-prediction rate at $\alpha = 1.16$ (13.9%) is only slightly smaller than the total false-prediction rate at $\alpha = 1$ (14.7%), we will continue to use Sheppard's model as in Eq. (1) ($\alpha = 1$) in the remainder of this paper.

d. Dependence of false predictions on nondimensional mountain height

Here, we examine the reasons for false predictions in more detail. To examine the distribution of false predictions as a function of nondimensional mountain height, Fig. 7 depicts the histogram of each type of prediction as a function of $U_\infty/(Nh)$ ($=1/h_{ND}$). The distributions are similar for day and night, and only the overall distributions are shown. Most of the observations for $U_\infty/(Nh) < 0.4$ (weak lifting) are correct negatives (no saturation). Correct positives become the larg-

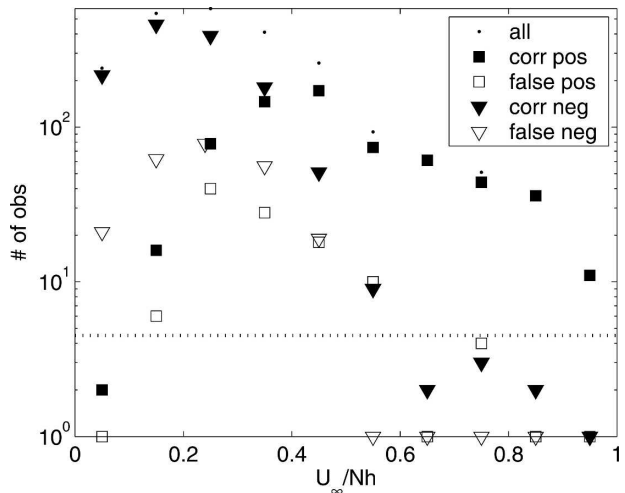


FIG. 7. Number of observations of correct positives, false positives, correct negatives, and false negatives as function of $U_\infty/(Nh)$. For clarity, bins with zero observations are shown as if they had one observation. For statistical convergence, only bins with more than five observations are considered for further study (horizontal line).

est fraction for $U_\infty/(Nh) > 0.4$ (moderate to strong lifting). False negatives (no saturation predicted but saturation observed) occur mostly in the small lifting range $U_\infty/(Nh) < 0.4$, because the predicted lifting must be small to obtain a no-saturation prediction. False positives (saturation predicted but not observed) occur for moderate lifting $0.2 < U_\infty/(Nh) < 0.5$, because the predicted lifting must be moderate to large for saturation to be predicted, whereas very strong lifting will always result in saturation even if the amount of lifting is slightly overpredicted. For this reason, correct positive predictions predominate in the strong lifting range [$U_\infty/(Nh) > 0.6$]. Further analyses (not shown) demonstrate that the data subsets consisting of false positives and false negatives differ from the full dataset in terms of wind speed: false negatives occur predominantly in weak winds ($U_\infty < 10 \text{ m s}^{-1}$), and false positives are mostly found for intermediate wind speeds ($5 < U_\infty < 15 \text{ m s}^{-1}$). In contrast, the Brunt-Väisälä frequency N has a much narrower range than does wind speed, and the frequency distributions of N in the full dataset, the subset of false positives, and the subset of false negatives are not significantly different. In a similar way, the frequency distributions of wind direction in the full dataset and the false-prediction subsets were not significantly different, as is expected because Pico Mountain is nearly axisymmetric at altitudes above 1200 m.

Based on the histograms in Fig. 7, only data bins with more than five observations are considered for further analysis in section 2e. Five 6-hourly observations correspond to more than 1 day of measurements.

TABLE 3. Differences between the measured θ_v at the mountaintop and θ_v at z_t from the ECMWF data.

Mean($\Delta\theta_v$) (K)	Day	Night
All	4.4	3.0
Correct negatives	4.0	1.9
False positives	4.3	3.3
Correct positives	5.8	5.5
False negatives	3.3	2.4

e. Analysis of the conservation of potential temperature and water vapor mixing ratio during uplift

It was shown in section 3a that Eq. (1) has high sensitivity and specificity for the prediction of water vapor saturation on the summit of Pico Mountain. In this section, we test Sheppard's model further by examining how well the conservation of virtual potential temperature θ_v and water vapor mixing ratio q holds along the streamline predicted by Eq. (1). This examination is done by evaluating the difference between the measured θ_v at the mountaintop and θ_v at z_t [as calculated by Eq. (1)]; that is, $\Delta\theta_v = \theta_{v,PICO} - \theta_v(z_t)$. Conservation of θ_v is only expected under conditions of negligible solar heating, no latent heat release, and no mixing during uplift. Thus the best agreement is expected for nighttime data without condensation (nighttime correct negatives and nighttime false positives).

We tested for offsets between the virtual potential temperatures in the ECMWF data and at the mountaintop by computing the average of $\Delta\theta_v$ for nighttime correct negatives in very weak lifting only [$U_\infty/(Nh) < 0.05$]. No offset was found, because $\Delta\theta_v$ was not significantly different from zero for this data subset. Table 3 shows $\Delta\theta_v$ as a function of the type of prediction. For the nighttime correct negatives and nighttime false positives, the mean differences are 1.9 and 3.3 K, respectively. These differences are statistically significantly greater than zero, and biases of these magnitudes are somewhat larger than those that would correspond to the median uplift errors deduced in section 3b. Higher temperatures on the mountaintop relative to those at the dividing-streamline height may be the result of turbulent mixing with higher and warmer air during uplift. A prediction bias such that the true z_t was from 190 (false positives) to 330 (correct negatives) m more than predicted could be an alternative to explain these values.

Figure 8 sheds more light on the dependence of $\Delta\theta_v$ on predicted lifting in daytime and nighttime. Correct negatives exhibit a $\Delta\theta_v$ of 2 K at nighttime for $U_\infty/(Nh) > 0.2$, with $\Delta\theta_v$ decreasing to zero for $U_\infty/(Nh)$ decreasing to zero. During the day, $\Delta\theta_v$ is constant around 4 K

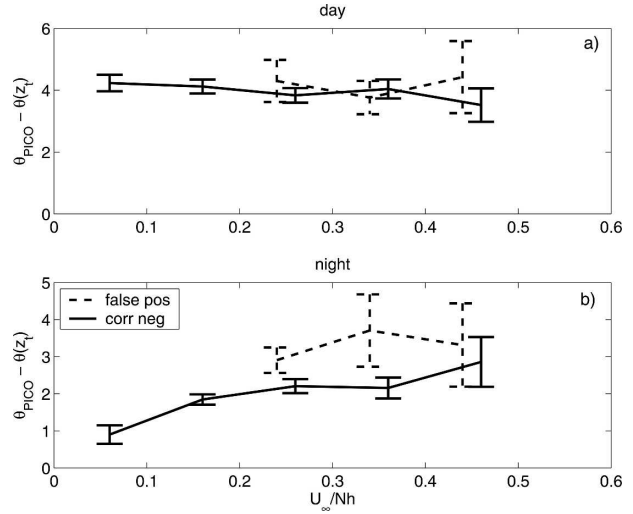


FIG. 8. Difference between the measured potential temperature at the mountaintop $\theta_{v,PICO}$ and θ_v at z_t [as calculated by Eq. (1)] for (a) daytime and (b) nighttime. Error bars indicate the 95% confidence interval on each mean.

for correct negatives and false positives. False positives experience a fairly constant offset $\Delta\theta_v$ of 3–4 K during nighttime. In summary, the difference $\Delta\theta_v$ is dependent on $U_\infty/(Nh)$ for small $U_\infty/(Nh)$ at night but is otherwise constant over the range of $U_\infty/(Nh)$ for all data subsets.

Consistent with this conclusion, linear fits to the false positive and correct negative nighttime data indicate slopes that are not significantly different from zero over the range $0.2 < U_\infty/(Nh) < 1$. A constant $\Delta\theta_v$ for $U_\infty/(Nh) > 0.2$ implies that Sheppard's model predicts the right increase in uplift with an increase in $U_\infty/(Nh)$. However, for $U_\infty/(Nh)$ increasing from 0 to 0.2, the actual uplift increases by less than is predicted by Sheppard's model. Assuming Sheppard's formula was valid, one would expect 450 m of lifting at $U_\infty/(Nh) = 0.2$, but the potential temperature comparison in Fig. 8 for correct negative data suggest that an uplift of only 250 m actually occurs, resulting in a $\Delta\theta_v$ of ~ 2 K.

For correct negatives (no saturation), daytime solar heating apparently accounts for 3 K in additional heating relative to nighttime for very small $U_\infty/(Nh)$. As $U_\infty/(Nh)$ increases to 0.5, the difference between daytime and nighttime becomes close to 1 K.

Water vapor should also be conserved during lifting in the absence of condensation or mixing. The results of an analysis of $\Delta q = q_{PICO} - q(z_t)$ are shown in Fig. 9. Because day–night differences were not observed for water vapor (in contrast to potential temperature), only a single plot showing all data is presented. A difference of $q = 1.45 \text{ g kg}^{-1}$ was found between ECMWF and the mountaintop station in very weak lifting [$U_\infty/(Nh) < 0.05$]. To evaluate conservation of q , only unsaturated

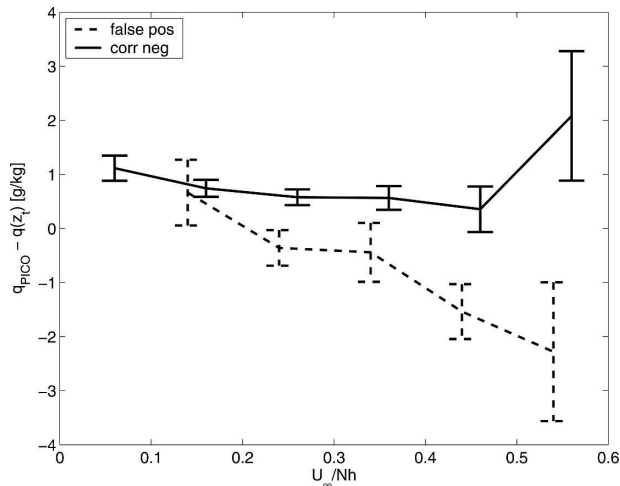


FIG. 9. Difference between the measured q at the mountaintop and q at z_t [as calculated by Eq. (1)]. Error bars indicate the 95% confidence interval on each mean.

data (false positives and correct negatives) should be used. Relative to the offset, the unsaturated data indicate higher humidity at z_t relative to the measured q_{PICO} : the difference Δq relative to the offset is significantly smaller than zero for all false-positive and correct-negative data points. As with virtual potential temperature conservation, for correct negatives the absolute value of Δq increased for $U_\infty/(Nh) < 0.2$, whereas the slope of data points with $U_\infty/(Nh) > 0.2$ was not significantly different from zero. However, for false positives the slope is significantly different from zero, even for $U_\infty/(Nh) > 0.2$. Because for false positives saturation was predicted but not observed, this increase in Δq could be related to inaccurate (positively biased) humidity values in the ECMWF data that contributed to the model error in this relatively small data subset.

4. Summary and conclusions

In this study, Sheppard's model for lifting was evaluated using sounding data created from numerical weather model output and field data obtained at the summit of a tall, steep mountain with nearly ideal axisymmetric shape.

By coupling Sheppard's airflow model [Eq. (1)] with thermodynamic calculations to determine the lifting condensation level of air originating from the dividing-streamline height z_t , water vapor saturation at the mountaintop was predicted and was compared with the observed relative humidity. These comparisons show that Sheppard's model is very successful in predicting saturation, with a false-prediction rate of 15%. An increase in lifting by 16% resulted in the lowest total false-prediction rate of 13.9%. This result implies that

the actual lifting for the data points whose LCL is close to the mountain height is slightly more than that predicted by Sheppard's formula.

In the ECMWF analysis, false positives (saturation predicted but no saturation observed) occur predominantly for intermediate wind speeds, and false negatives occur in weak winds. If Sheppard's formula is assumed to be valid and the reason for false predictions is assumed to be related to uncertainties in the input data, a 38% standard deviation in the predicted lifting would explain the false predictions. However, errors in the model prediction can also be explained by deficiencies in Sheppard's model. The flow over the mountain is influenced by turbulent mixing, pressure forces, and temperature differences between the mountain and the overlying air, none of which are taken into account by the model.

In comparing potential temperature and water vapor mixing ratio at the dividing-streamline height z_t in the sounding to the mountaintop measurements, it was found that the air at z_t is colder and moister than at the mountaintop, even at night in unsaturated conditions. This situation could mean that the dividing-streamline height is underpredicted (i.e., lifting is overpredicted) by Sheppard's model. On the other hand, turbulent mixing with higher-altitude air during ascent may contribute to this difference. Near the mountain, the convergence of streamlines and the resulting wind shear may lead to mixing of higher (cooler and drier) air into air on the dividing streamline.

There is an apparent inconsistency between the analysis in section 3c, in which more uplift would have slightly decreased the number of false predictions, and the analysis in section 3e, in which less uplift would have resulted in better conservation of potential temperature and water vapor mixing ratio. However, the analysis in section 3c was most influenced by data points for which LCL was close to the mountain height (a small data subset), whereas the analysis in section 3e was dominated by a much larger dataset (all correct-negative and false-positive predictions).

Of interest is that the absolute value of the differences in potential temperature and water vapor mixing ratio increased for $U_\infty/(Nh) < 0.2$ but did not significantly vary over the range $U_\infty/(Nh) > 0.2$. This result indicates that Sheppard's model underpredicts the amount of uplift for weak wind speeds but predicts the relative increase in uplift with increasing $U_\infty/(Nh)$ correctly.

We conclude that for important practical applications such as prediction of mountain clouds Sheppard's formula quantified lifting on Pico Mountain accurately. The results are consistent with experimental and nu-

merical studies (Ding et al. 2003; Vosper et al. 1999) that found that Sheppard's formula predicts the dividing-streamline height correctly, with a slight tendency to overpredict the degree of lifting. The results also help to explain the good performance of Leung and Ghan's (1995) simple parameterization based on Sheppard's model to determine orographic precipitation.

Future research should focus on obtaining more detailed field data upstream and on the slope of a near-axisymmetric tall mountain such as Pico Mountain to address issues such as the thermodynamic evolution of a fluid parcel during ascent and the influence of turbulent mixing on the thermodynamic properties. In addition, liquid water measurements at the mountaintop would allow for an improved analysis of potential temperature and water vapor mixing ratio conservation. Our cloud forecast model has been used in supporting operations at the PICO-NARE station—for example, to plan helicopter airlifts and to support decisions regarding the safety of hiking on the mountain. It may be valuable to apply Sheppard's model as a cloud prediction tool in an operational forecast for other mountain peaks that are unresolved or underresolved by numerical weather models.

Acknowledgments. The authors thank Michael Dziohak, María Val Martín, and R. Chris Owen for their efforts to keep the PICO-NARE station running in adverse weather conditions. The authors gratefully acknowledge funding from NOAA Grants NA16GP1658 and NA03OAR4310002.

REFERENCES

- Baines, P. G., 1995: *Topographic Effects in Stratified Flows*. Cambridge University Press, 482 pp.
- , and R. B. Smith, 1993: Upstream stagnation points in stratified flow past obstacles. *Dyn. Atmos. Oceans*, **18**, 105–113.
- Barros, A. P., and D. P. Lettenmaier, 1994: Dynamic modeling of orographically induced precipitation. *Rev. Geophys.*, **32**, 265–284.
- Bougeault, P., and Coauthors, 2001: The MAP special observing period. *Bull. Amer. Meteor. Soc.*, **82**, 433–462.
- Carbone, R. E., W. A. Cooper, and W.-C. Lee, 1995: Forcing of flow reversal along the windward slopes of Hawaii. *Mon. Wea. Rev.*, **123**, 3466–3480.
- Chen, Y.-L., and A. J. Nash, 1994: Diurnal variations of surface airflow and rainfall frequencies on the island of Hawaii. *Mon. Wea. Rev.*, **122**, 34–56.
- Colville, R. N., and Coauthors, 1997: Meteorology of the Great Dun Fell cloud experiment 1993. *Atmos. Environ.*, **31**, 2407–2420.
- Ding, L., R. J. Calhoun, and R. L. Street, 2003: Numerical simulation of strongly stratified flow over a three-dimensional hill. *Bound.-Layer Meteor.*, **107**, 81–114.
- Drazin, P. G., 1961: On the steady flow of a fluid of variable density past an obstacle. *Tellus*, **13**, 239–251.
- Grisogono, B., and L. Enger, 2004: Boundary-layer variations due to orographic wave-breaking in the presence of rotation. *Quart. J. Roy. Meteor. Soc.*, **130**, 2991–3014.
- Heinold, B., A. Tilgner, W. Jaeschke, W. Haunold, O. Knoth, R. Wolke, and H. Herrmann, 2005: Meteorological characterization of the FEBUKO hill cap cloud experiments, part II: Tracer experiments and flow characterisation with nested non-hydrostatic atmospheric models. *Atmos. Environ.*, **39**, 4195–4207.
- Honrath, R. E., and Coauthors, 2004: Regional and hemispheric impacts of anthropogenic and biomass burning emissions on summertime CO and O₃ in the North Atlantic lower free troposphere. *J. Geophys. Res.*, **109**, D24310, doi:10.1029/2004JD005147.
- Hunt, J. C. R., and W. H. Snyder, 1980: Experiments on stably and neutrally stratified flow over a model three-dimensional hill. *J. Fluid Mech.*, **96**, 671–704.
- Jenkins, G. J., P. J. Mason, W. H. Moores, and R. I. Sykes, 1981: Measurements of the flow structure around Ailsa Craig, a steep, three-dimensional, isolated hill. *Quart. J. Roy. Meteor. Soc.*, **107**, 833–851.
- Jiang, Q., 2003: Moist dynamics and orographic precipitation. *Tellus*, **55A**, 301–326.
- Leung, L. R., and S. J. Ghan, 1995: A subgrid parameterization of orographic precipitation. *Theor. Appl. Climatol.*, **52**, 95–118.
- Miglietta, M. M., and A. Buzzi, 2001: A numerical study of moist stratified flows over isolated topography. *Tellus*, **53A**, 481–499.
- Olafsson, H., and P. Bougeault, 1996: Nonlinear flow past an elliptic mountain ridge. *J. Atmos. Sci.*, **53**, 2465–2489.
- Perry, S., and Coauthors, 1989: User's guide to the complex terrain dispersion model plus algorithms for unstable situations (CTDMPLUS). EPA, 210 pp.
- Sheppard, P. A., 1956: Airflow over mountains. *Quart. J. Roy. Meteor. Soc.*, **82**, 528–529.
- Smith, R. B., 1980: Linear theory of stratified hydrostatic flow past an isolated mountain. *Tellus*, **32**, 348–364.
- , 1988: Linear theory of stratified flow past an isolated mountain in isosteric coordinates. *J. Atmos. Sci.*, **45**, 3889–3896.
- , 1989: Mountain-induced stagnation points in hydrostatic flow. *Tellus*, **41A**, 270–274.
- , and S. Gronas, 1993: Stagnation points and bifurcation in 3-d mountain airflow. *Tellus*, **45A**, 28–43.
- , and I. Barstad, 2004: A linear theory of orographic precipitation. *J. Atmos. Sci.*, **61**, 1377–1391.
- Smolarkiewicz, P. K., and R. Rotunno, 1990: Low Froude number flow past three-dimensional obstacles. Part II: Upwind flow reversal zone. *J. Atmos. Sci.*, **47**, 1498–1511.
- Snyder, W. H., 1985: Fluid modeling of pollutant transport and diffusion in stably stratified flows over complex terrain. *Annu. Rev. Fluid Mech.*, **17**, 239–266.
- Spangler, T. C., 1987: Comparison of actual dividing-streamline heights to height predictions using the Froude number. *J. Climate Appl. Meteor.*, **26**, 204–207.
- Taylor, P. A., and H. W. Teunissen, 1987: The Askervein hill project: Overview and background data. *Bound.-Layer Meteor.*, **39**, 15–39.
- Trombetti, F., and F. Tampieri, 1987: An application of the dividing-streamline concept to the stable airflow over mesoscale mountains. *Mon. Wea. Rev.*, **115**, 1802–1806.
- Vosper, S. B., I. P. Castro, W. H. Snyder, and S. D. Mobbs, 1999: Experimental studies of strongly stratified flow past three-dimensional orography. *J. Fluid Mech.*, **390**, 223–249.